

Received 19 November 2021

Accepted 18 January 2022

Edited by M. Spackman, University of Western
Australia, Australia**Keywords:** biogenic calcite; X-ray diffuse scattering; inelastic X-ray scattering; mechanical properties.

Mesocrystalline structure and mechanical properties of biogenic calcite from sea urchin spine

Helmut Cölfen,^a Hans-Beat Bürgi,^{b,c} Dmitry Chernyshov,^d Michal Stekiel,^e
Aleksandra Chumakova,^f Alexei Bosak,^{f,*} Björn Wehinger^f and Bjoern Winkler^g

^aPhysical Chemistry, Department of Chemistry, University Konstanz, Universitaetsstrasse 10, Konstanz 78457, Germany, ^bDepartment of Chemistry, University of Zürich, Winterthurerstrasse 190, Zürich, CH-8057, Switzerland, ^cDepartment of Chemistry, Biochemistry and Pharmacy (DCBP), Universität Bern, Freiestrasse 3, Bern, CH-3012, Switzerland, ^dSwiss-Norwegian Beam Lines at the European Synchrotron Radiation Facility, 71 Avenue des Martyrs, Grenoble 38000, France, ^eDepartment of Physics, Technical University Munich, James-Franck-Strasse 1, Garching 85748, Germany, ^fEuropean Synchrotron Radiation Facility, 71 Avenue des Martyrs, Grenoble 38000, France, and ^gInstitute of Geosciences, Goethe University Frankfurt, Altenhoferallee 1, Frankfurt am Main 60438, Germany. *Correspondence e-mail: bossak@esrf.fr

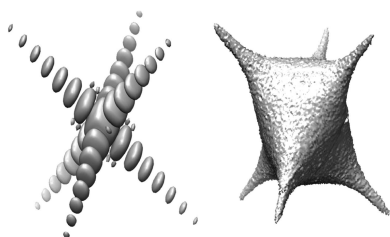
Using X-ray scattering, we measured detailed maps of the diffuse scattering intensity distribution and a number of phonon dispersion branches for a single crystal of inorganically formed natural calcite and for high-quality mesocrystals of biogenic calcite from a Mediterranean sea urchin spine. A comparison shows that the known differences in the mechanical properties between the ‘strong’ biogenic and ‘brittle’ abiotic material should be attributed to the mesoscopic architecture of the crystal rather than to a modification of the calcite crystal structure. The data are rationalized by comparing them to the results of *ab initio* model calculations of lattice dynamics. For the mesocrystal, they are augmented by the evaluation of the faceting of the constituent nanocrystals.

1. Introduction

Biomateriality is a rapidly expanding domain of knowledge dealing with mineral phases produced by living species for mechanical support, protection, defence and other purposes. Depending on phyla, a variety of minerals can be found; here, we focus on biogenic calcium carbonate (Addadi & Weiner, 1997). Sea urchins are known to have both spines and dents consisting of single crystals of carbonates interspersed with proteinaceous domains (Weiner *et al.*, 2000). Sea urchin spines have been optimized by nature for at least 450 million years, and we would like to know whether this optimization concerns the mesoscopic protein/mineral architecture only or includes the design of the crystalline material as well, *e.g.* by doping or ordering. Calcites of biological origin show anisotropically distorted unit-cell parameters (Zolotoyabko & Pokroy, 2007) and ~50% increased atomic displacement parameters (ADPs) (Magdanas & Gies, 2004) compared to inorganically formed natural or synthesized calcite (Markgraf & Reeder, 1985).

2. Experimental

X-ray diffuse scattering maps were collected at the ID23 beamline at the European Synchrotron Radiation Facility. The measurements were performed in shutterless mode with a wavelength of 0.7749 Å and a beam spot of ~50 µm × 50 µm on the sample. Diffraction images were collected by performing φ scans with 0.1° steps in the $\varphi = \pm 180^\circ$ range. Inelastic X-ray scattering (IXS) measurements were performed at the ID28 spectrometer (Krisch & Sette, 2007),



operating at 0.6968 Å and providing an instrumental energy resolution of 3 meV. An intact spine of *Paracentrotus lividus* (~1 mm diameter) was used for the IXS experiment and an optically uniform sector fragment without apparent porosity was isolated for the diffuse scattering study (~0.2 mm). The expected Mg content is of the order of a few percent (3.7% reported for the same species before; McClintock *et al.*, 2017).

2.1. Computational details

Density functional theory (DFT)-based atomistic model calculations have been employed for the parameter-free calculation of phonon frequencies and displacement patterns. Details of the calculations were presented previously (Stekiel *et al.*, 2019), where the excellent agreement of the lattice dynamic calculations with experimentally obtained dispersion curves and diffuse scattering distributions has been used to understand phase transitions in carbonates.

3. Results and discussion

The intensity maps obtained here for inorganically formed natural calcite contain a large number of distinct features, which can be fully rationalized as thermal diffuse scattering and hence are reproduced by the atomistic *ab initio* models (Fig. 1, left column). The diffuse clouds around the Bragg nodes are more isotropic for biogenic than for abiotic calcite.

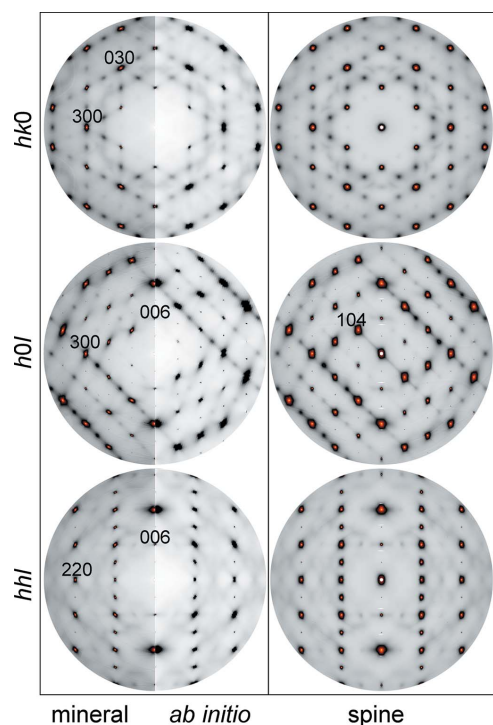


Figure 1

Diffuse scattering intensity maps for inorganically formed natural calcite in comparison to *ab initio* calculations [left column; for experimental and computational details see Bosak *et al.* (2015)] and for sea urchin spine (right column). Laue symmetry elements are applied to the reconstructed maps in order to remove the detector gaps. Combined linear greyscale/logarithmic colour scale visualization is applied to the experimental data.

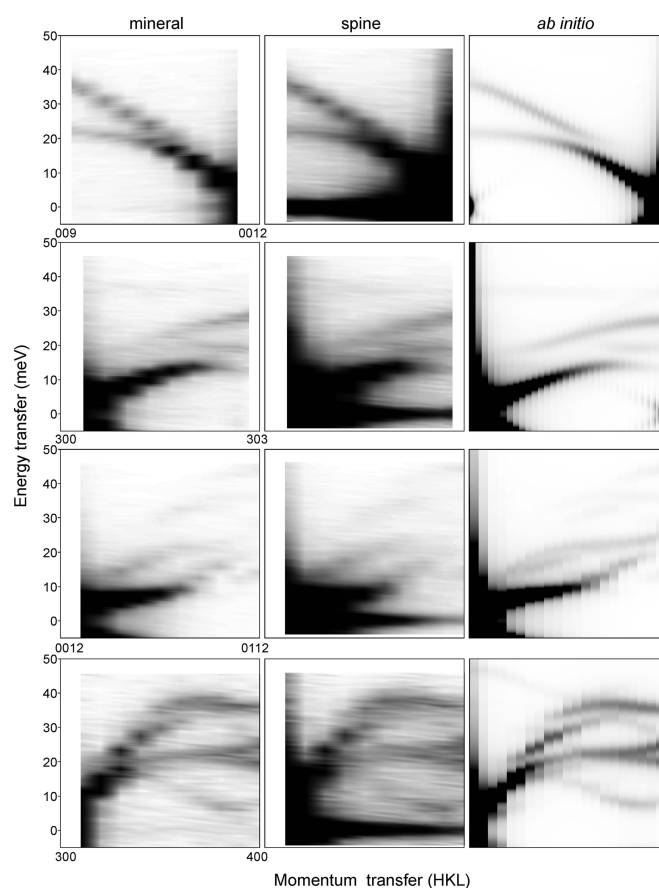


Figure 2

Linear greyscale intensity maps in (Q - E) coordinates, measured for abiotic (left column) and biogenic (middle column) calcite, compared to the *ab initio* calculated dynamical structure factor (right column). Data are scaled for visualization purposes: zero intensity is mapped to white and saturation cut-off to black.

In addition, a significant amount of anisotropic small-angle scattering is observed in the central parts of the reconstructed images of the spine. The change of the anisotropy of the diffuse clouds in the proximity of the Bragg nodes can be due to a change of elastic moduli or to the appearance of an extra component of diffuse scattering. The inelastic scattering experiment can unambiguously resolve the origin, as it separates the phonon component (which is related to the elasticity) from the defect-related contribution.

Inelastic scattering data for a few representative directions are shown as intensity maps in momentum transfer–energy (Q - E) coordinates in Fig. 2. The scattering intensity of inorganically formed natural calcite (left column) vanishes at zero energy transfer, and its dynamical structure factor reliably corresponds to the results of the *ab initio* calculations (right column). The latter have been calculated with an established formalism (Bosak *et al.*, 2015) using phonon eigenvalues and eigenvectors from Stekiel *et al.* (2019). Intensity maps for the sea urchin spine (middle column) show essentially identical phonon dispersions and do not contain any extra features, except for a divergence of the intensity of the elastic line towards the Brillouin zone centre (zero reduced momentum transfer).

Since the phonon contributions into diffuse scattering patterns are practically the same, the difference in diffuse scattering has to be attributed to a static disorder. Variations of Ca/Mg composition and associated displacements, and fluctuations in shape and size of the structurally coherent volumes serve as the main components of the static disorder in biocalcite. In terms of the average structure, the static disorder smears out the scattering density and the smearing is normally parameterized with ADPs. Thus, a ~50% increase in ADPs for biocalcite compared to the synthetic analogue (Magdans & Gies, 2004) can be attributed to static disorder but not to the difference in the vibrational spectra.

The intrinsic elasticity of biogenic calcite is thus hardly distinguishable from that of abiotic natural calcite. The elastic diffuse scattering from biogenic calcite, clearly visible near the centres of its diffuse scattering maps, *i.e.* at the origin of reciprocal space, can be interpreted in terms of small-angle scattering originating from the shapes of mesoscale crystallites. In practice, qualitatively, the shape of diffuse clouds can be reproduced as a sum of thermal diffuse scattering characteristics for the given node with the properly scaled small-angle scattering corresponding to the shape function of individual crystallites. It is compatible with truncation of the crystallites by {104}-type planes, which are low energy cleavage planes. Fig. 3 illustrates the shape function (power spectrum of the crystal shape) of an equilateral crystal; real spine domains are neither equilateral nor monodisperse, but the anisotropic envelope of their shape functions with diffuse tails protruding along 104 is conserved (to be compared with the $h0l$ section in Fig. 1), while interference ripples are lost. Nanoscale faceting with {104} facets derived from the diffuse scattering perfectly corresponds to the electron micrographs taken for similar samples (Seto *et al.*, 2012).

4. Conclusions

The inelastic scattering component is very similar for single-crystal abiotic natural calcite and sea urchin spine, which implies a close similarity of the elastic stiffness coefficients. The difference in material strength between biogenic and abiotic natural calcite thus originates from the mesoscopic structure, as detailed by Seto *et al.* (2012), and the difference in diffuse scattering is due to a mesoscale structure with {104} nanofaceting of biogenic calcite crystals. A detailed study of diffuse scattering combined with small-angle scattering for different subclasses of *Echinoidea* should be performed both for spines and for the individual calcite plates of the internal skeleton to confirm and extend the insight gained in the present study. The unique micromechanical properties of sea urchin spines are likely related to their intricate mesoscopic structure and microscopic architecture (Tsafnat *et al.*, 2012), rather than to modification of the microscopic properties of their component calcite crystallites. The highly porous single-

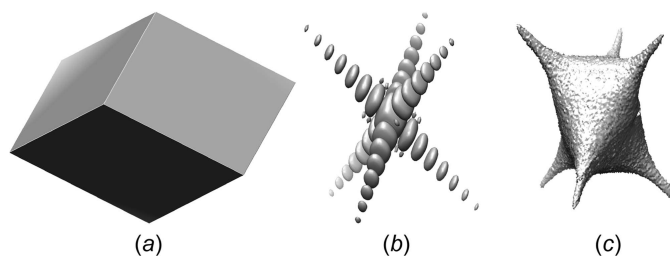


Figure 3

(a) Equilateral calcite rhombohedron with {104} faceting; (b) power spectrum of such a crystal in isointensity surface representation; (c) isointensity surface representation of small-angle scattering on sea urchin spine – tails are pointing towards 104 spots. Real space and reciprocal space scales are arbitrary and frame orientation is selected to be the same.

crystal material of spines with developed mesoscale structure may also be considered as a prototype of a new lightweight construction materials developed by nature (Presser *et al.*, 2009).

Acknowledgements

The authors are grateful to A. Popov and D. Flot (ESRF) for offering access to the diffraction beamline. BW is grateful for financial support through the DFG–Research Unit DFG–FOR2125 ‘CarboPaT’ and for support through the BIOVIA Science Ambassador Program.

Funding information

Funding for this research was provided by: Deutsche Forschungsgemeinschaft (grant No. DFG-FOR2125 ‘CarboPaT’ to BW).

References

- Addadi, L. & Weiner, S. (1997). *Nature*, **389**, 912–913.
- Bosak, A., Chernyshov, D., Wehinger, B., Winkler, B., Le Tacon, M. & Krisch, M. (2015). *J. Phys. D Appl. Phys.* **48**, 504003.
- Krisch, M. & Sette, F. (2007). *Inelastic X-ray Scattering from Phonons*, in *Light Scattering in Solids, Novel Materials and Techniques*, Vol. 108, *Topics in Applied Physics*. Springer-Verlag.
- Magdans, U. & Gies, H. (2004). *Eur. J. Mineral.* **16**, 261–268.
- Markgraf, S. A. & Reeder, R. J. (1985). *Am. Mineral.* **70**, 590–600.
- McClintock, J., Amsler, M., Angus, R., McClintock, F., Geneviere, A.-M. & Lebrato, M. (2017). *Cah. Biol. Mar.* **58**, 99–106.
- Presser, V., Schultheiß, S., Berthold, C. & Nickel, K. G. (2009). *J. Bionic Eng.* **6**, 203–213.
- Seto, J., Ma, Y., Davis, S. A., Meldrum, F., Gourrier, A., Kim, Y.-Y. & Cölfen, H. (2012). *PNAS*, **109**, 3699–3704.
- Stekiel, M., Girard, A., Nguyen-Thanh, T., Bosak, A., Milman, V. & Winkler, B. (2019). *Phys. Rev. B*, **99**, 054101.
- Tsafnat, N., Fitz Gerald, J. D., Le, H. N. & Stachurski, Z. H. (2012). *PLoS One*, **7**, e44140.
- Weiner, S., Addadi, L. & Wagner, H. D. (2000). *Mater. Sci. Eng. C*, **11**, 1–8.
- Zolotoyabko, E. & Pokroy, B. (2007). *CrystEngComm*, **9**, 1156–1161.